Chapter 4

Simulation of electrohydrodynamic flows

Electrohydrodynamics is a wide class of phenomena in liquids and gases placed in electric field in contact with electrodes. On the electrode surface, charge injection and various electrochemical reactions can occur (later ones can also happen in the bulk of fluid). The electric field exerts a force on the charged particles, at the same time, electric charge changes the spatial distribution of the electric potential. Electrodynamic forces can produce flows of fluid, these flows lead to charge transport.

The breakdown of dielectrics occurs at sufficiently high electric field strength. The breakdown proceeds in several stages. At first, one or several luminous formations appear near one of electrodes. The time between the voltage application and the appearance of such formations is called the statistical lag time, it can be different in subsequent experiments. Depending on conditions, different mechanisms of the breakdown inception are possible: the bubble mechanism, the thermal one, the ionization one, etc.

At the next stage of breakdown, conductive channels (called streamers) grow from the formations appeared to the opposite electrode. Streamers have usually a dendrite-like shape and they can also branch. Patterns of streamer structure are stochastic enough and the structure is not reproduced exactly in subsequent experiments. The electric conductivity inside streamers is sufficiently high, hence, the energy is released there leading to expansion of streamers. Divergent shock waves and flows of liquid arise around each expanding channel. Waves from different streamer channels interact, that additionally complicates the flow pattern. The back-influence of compression waves upon the dynamics of streamer channels is also possible.

When one of streamers reaches the opposite electrode, the last stage of the electric discharge in liquid — the channel one — begins. The energy is released

at the passing of the electric current, the channel expands generating a divergent shock wave. A flux of fluid into the channel through its boundary exists, this fluid is converted to the channel plasma after dissociation and ionization.

Simulation of electrohydrodynamic flows is a complicated problem where one should take into account many concurrent phenomena. In this chapter, flows at a low electric field and the bubble generation near electrodes are considered. Streamer dynamics and flows at the channel stage of electric discharge are considered in chapter 5.

The LBE method with 9 possible velocity vectors on a square lattice ($|c_k| =$ 0, 1 and $\sqrt{2}$) was used in computations of this chapter. To simulate EHD flows, one should incorporate properly the electrohydrodynamic effects [8]:

1. Convective charge transport by moving liquid;
2. Charge transport by conductivity currents, the computation of the electric potential is necessary;
3. Effect of the electrodynamic forces on charged liquid being in electric field.

4.1 Computation of charge transport

The electric charge in a node is changed due to the convective transport of charge by moving liquid and due to the conductivity currents (electric drift of electrons and ions). Below, these mechanisms are considered separately.

4.1.1 Convective charge transport

Equation of the convective charge transport follows from the charge conservation law. This equation is given by:

$$\partial q/\partial t = -\mathrm{div}(q\mathbf{u}).$$

Here q is the charge density, $\mathbf{u}$ is the velocity of liquid. Three methods were used to solve this equation: the method of "LBE-particles", the method of mean velocity and the method of additional LBE component.

In the method of "LBE-particles", the part of node charge $q_k = qN_k/\rho$ is passively transported to the neighbor node along the k-th lattice link. This method results in numeric diffusivity of $D_1 = c_s^2\Delta t/2$. In particular, for the two-dimensional model with 9 directions, one obtains $c_s = h/\sqrt{3}\Delta t$ and $D_1 = h^2/6\Delta t$.

Example of computations is shown in fig. 4.1. There were initial density discontinuity in the middle of the computation cell, the liquid velocity was initially

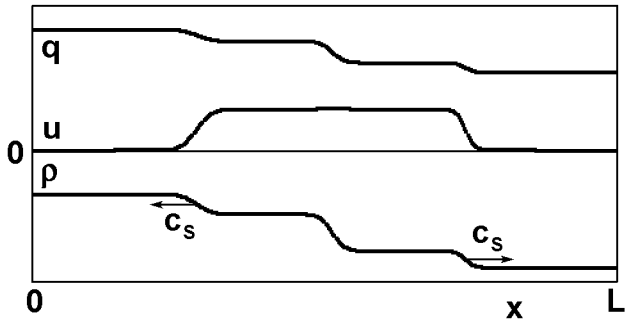

Figure 4.1. Liquid flow and charge distribution at zero conductivity in the absence of electrodynamic forces

zero. The initial charge density was everywhere proportional to the liquid density. The decay of discontinuity occured, a shock wave and a rarefaction wave were generated. The charge distribution coincides with the density distribution (charge is "frozen" into the liquid).

This method is clearly unacceptable for uniform liquid, however, it can be used to compute the dynamics of conductive inclusions, if in two-component medium only one component can carry electric charge.

The method of mean velocity is based on finite-difference method. For the one-dimensional case, the equations are given by:

$$\frac{q^{n+1}-q^n}{\Delta t} = \frac{1}{2h}\left(q^n_{i-1}(u_{i-1/2}+|u_{i-1/2}|) - q^n_{i+1}(u_{i+1/2}-|u_{i+1/2}|)\right.$$
$$\left. -q^n_i(u_{i+1/2}+|u_{i+1/2}|+u_{i-1/2}-|u_{i-1/2}|)\right),$$

where $u_{i+1/2} = (u_i + u_{i+1})/2$. The numeric diffusivity for this method is $D_2 = \frac{|u|(h/\Delta t - |u|)}{2}$, it depends on flow velocity. Maximum of diffusivity is $D_2|_{max} = h^2/8\Delta t$ for $u_m = h/2\Delta t$, it is lower than D_1. A flow velocity is usually much lower than u_m, it additionally diminishes D_2 comparing to $D_2|_{max}$.

The formulas for diffusivity of both methods were tested for the case of a one-dimensional liquid flow with constant velocity u_0 by comparison of numerical results with the well-known exact solution for the diffusion equation

$$q(x) = \frac{Q}{\sqrt{4\pi Dt}} \exp\left(-\frac{(x-u_0 t)^2}{4Dt}\right)$$

with the charge Q initially located at the point $x = 0$. For all velocities within the stability range of the LBE method, the numerical results coincided completely with the exact solution.

In the method of additional LBE component, the charge transport is simulated as the transport of passive scalar (see chapter 1). In this case, the charge diffusivity is $D_3 = \frac{h^2}{3\Delta t^2}(\tau_n - \frac{\Delta t}{2})$, it depends on the relaxation time τ_n, and it can be chosen independent on the properties of liquid.

Test computations were carried out of the liquid flow with charge transfer for different values of charge diffusivity D_3. Results are shown in fig. 4.2.

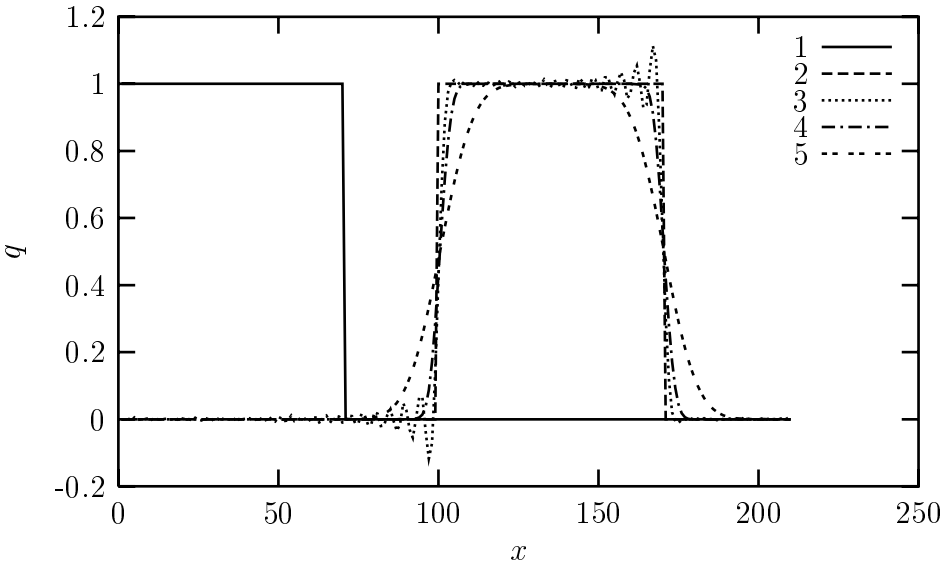

Figure 4.2. Transformation of charge distribution in one-dimensional liquid flow in the case of zero electric conductivity. The velocity of uniform flow was $u_0 = 0.1$. Initial charge distribution (curve *1*); theoretical charge distribution without diffusion (*2*) at $t = 1000$. Computed charge distribution at $t = 1000$ for the diffusivity $D_3 = 3.3(3) \cdot 10^{-4}$ (*3*); $D_3 = 3.3(3) \cdot 10^{-3}$ (*4*) and $D_3 = 3.3(3) \cdot 10^{-2}$ (*5*)

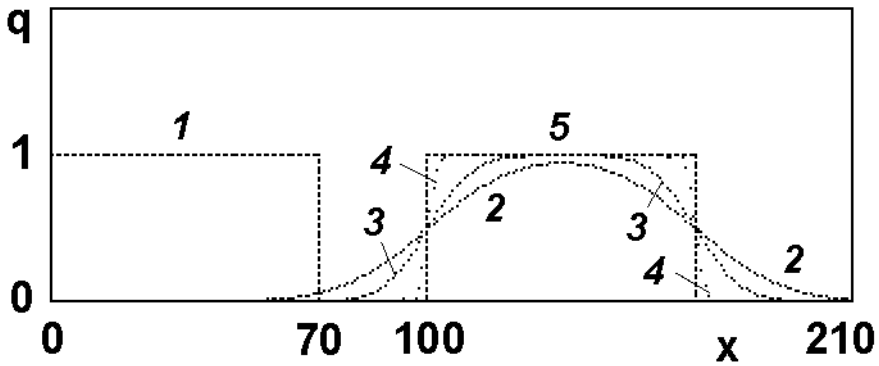

Figure 4.3. Transformation of charge distribution in uniform liquid flow in the case of zero electric conductivity

Electric charge was initially uniformly distributed $q(x) = q_0$ in a region $x_1 < x < x_2$. The liquid flow was uniform with constant velocity $u = u_0$ equal to 0.1. Boundary conditions were periodic. The good agreement with theoretical distribution is clear. At too low values of D_3, oscillations of charge density were observed in regions of high gradients (fig. 4.2, curve 3).

Results of computation of the convective charge transport are shown in fig. 4.3, here the initial and boundary conditions are the same as in fig. 4.2. Curve 1 presents the initial charge distribution. Computation results for the method of "LBE-particles" (curve 2), the method of mean velocity(curve 3) and the method of additional LBE component (curve 4), all for $t = 1000$, are

also shown. Curve 5 is the theoretical charge distribution without diffusion for $t = 1000$. Diffusivities were $D_1 = h^2/6\Delta t$ for the method of "LBE-particles", $D_2 = 0{,}045h^2/\Delta t$ for the method of mean velocity, and $D_3 = 0{,}0033h^2/\Delta t$ for the method of additional LBE component.

Thus, the method of the additional LBE-component allows one to reduce numeric diffusivity by more than order of magnitude comparing with previous methods.

4.1.2 Conductivity currents

The equation of conductive charge transport $\partial q/\partial t = -\mathrm{div}\,\mathbf{j} = -\mathrm{div}(\sigma\mathbf{E})$ was solved together with Poisson's equation for the electric potential $\Delta\varphi = -4\pi q$ by time-implicit finite-difference scheme of [100]. The conduction of each bond was calculated using the expression $G_{ij} = \sigma_0 h\sqrt{n_i n_j}$, where σ_0 is the liquid conductivity, n_i, n_j are the concentrations of the conductive phase at the edges of the bond, h is the lattice unit. This expression ensures electric charge transfer by current only inside the region occupied by the conductive phase. The conductivity of liquids used in EHD apparatuses is usually small. Moreover, it was shown in [101] that in the planar case the charge drift is negligible comparing to the convective charge transport. Therefore, bulk liquid conductivity was assumed zero in following computations. To simulate charge injection, certain conductivity was assigned at layers adjacent to electrodes.

4.2 Electrodynamic forces

Along with charge transfer, the action of electrodynamic forces on a liquid should be taken into account (just these forces are the cause of flow onset). The electrodynamic force acting on the electric charge q at a node is given by $\mathbf{F} = q\mathbf{E} = -q\nabla\varphi$. In the finite-difference form, the cartesian components of the force are $F_x = -q(\varphi_{i+1,j} - \varphi_{i-1,j})/2h$, $F_y = -q(\varphi_{i,j+1} - \varphi_{i,j-1})/2h$. Use of the centered form for the derivative eliminates the contribution of the node charge to the electric field (i.e., the self-action of charge). The action of the electrodynamic force leads to a change of momentum at a node by $\Delta\mathbf{p} = \mathbf{F}\Delta t$, corresponding velocity change is $\Delta\mathbf{u} = \Delta\mathbf{p}/\rho$. The modified velocity was used in the collision operator of the LBE method (equilibrium distribution functions are computed based on the velocity $\mathbf{u}' = \mathbf{u} + \Delta\mathbf{u}$). Thus, the action of the electric field on a charged liquid is computed.

Computation results of one-dimensional liquid flow are presented in fig. 4.4. The liquid flow was simulated by the LBE on a square lattice with 4 values of

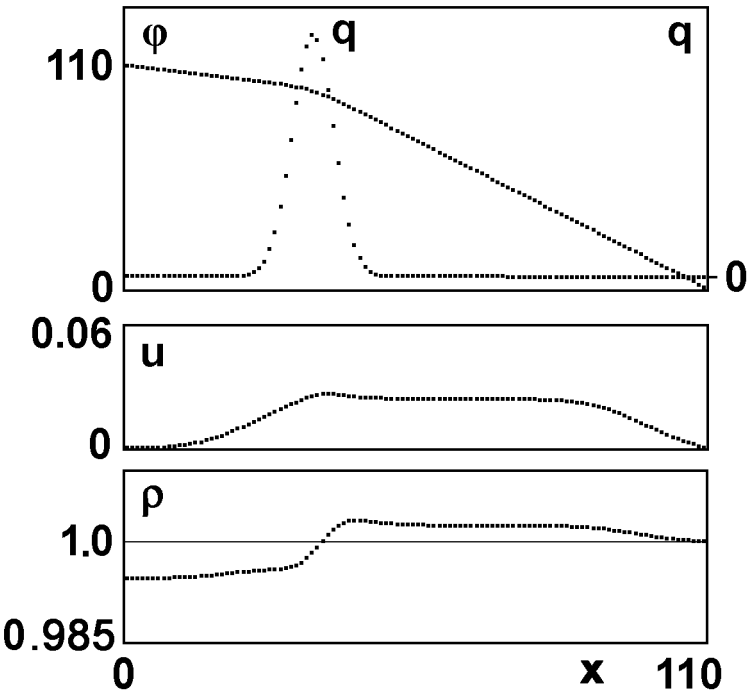

Figure 4.4. Liquid flow and charge distribution. $\varphi_0 = 110$, $Q = 0.08$, $x_0 = 36$, $L = 110$, $t = 70$, $\rho_0 = 1$

velocity (see. fig. 1.4,*b*). The positive charge Q was initially distributed along X coordinate according to the function

$$q(x) = \frac{Q}{\sqrt{2\pi b^2}} \exp\left(-\frac{(x - x_0)^2}{2b^2}\right),$$

charge density was constant along vertical lines. Boundary conditions for Poisson's equation were $\varphi = 0$ at $x = L$, $\varphi = \varphi_0$ at $x = 0$. Left and right boundaries were rigid walls. The charge began to move to the right under the action of electric field, generating the rarefaction wave moving to the left, and the compression wave moving to the right. At the time instance presented in the figure, the rarefaction wave had already reflected from the left wall.

4.3 Two-dimensional EHD flow (EHD-pump)

The EHD flow in two dimensional blade–plane geometry was considered. Computations were carried out in a square cell of size of 106×106 lattice sites between two plane electrodes at the top and bottom. Boundary conditions along the X axis were periodic. The electric potential of the upper electrode was zero, of the lower one it was $\varphi_0 = 106$, hence, the average field in the region was $E_a = 1$. In the middle of the lower electrode, a rectangular protrusion was placed of size of 5×2. The charge injection was possible from the top of the protrusion (conductivity of adjacent liquid layer was $\sigma_0 = 2 \cdot 10^{-4}$).

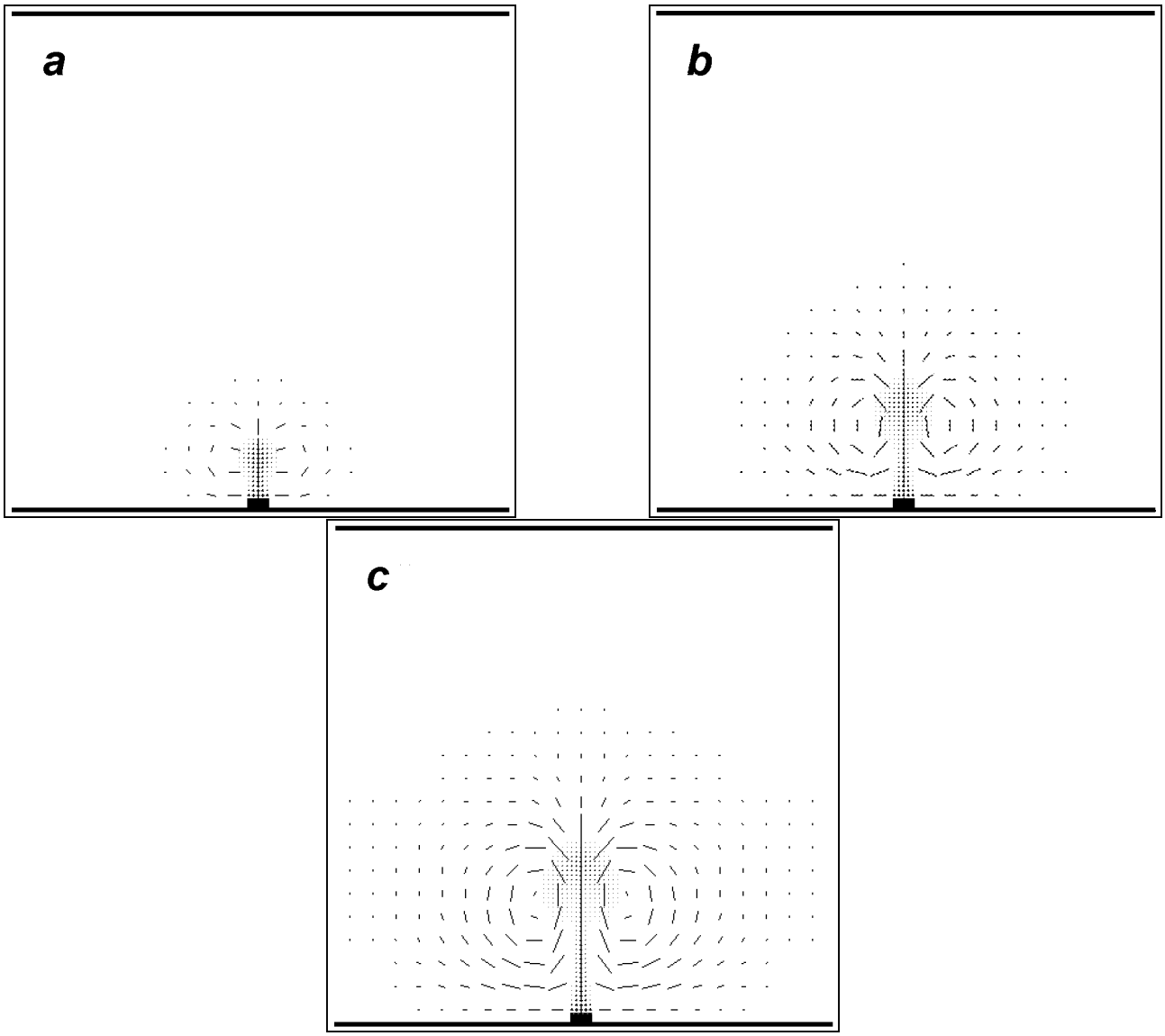

Figure 4.5. Two-dimensional EHD low. Velocity field (shown by lines) and charge density (shown by shades of gray). Time is $t = 275$ (a), $t = 400$ (b), $t = 510$ (c)

Figure 4.5 shows the flow development. When the voltage was applied, the charge injection began from the protrusion. Then a charged lump began to move upwards due to the action of electric field. The liquid flow in the form of vortical dipole was formed. The extent of region of moving liquid and the velocity magnitude grew in time. The maximal velocity in computations was about 0.05. Because of the increase in the "head" of the charged jet, the electric field on the top of the protrusion decreased and further injection was reduced. Development of conductive structures of such type was observed in experiments on the breakdown of highly viscous dielectrics [102], and at certain regimes of the partial breakdown [103].

In this example, no charge sink existed, hence, charge accumulation and flow

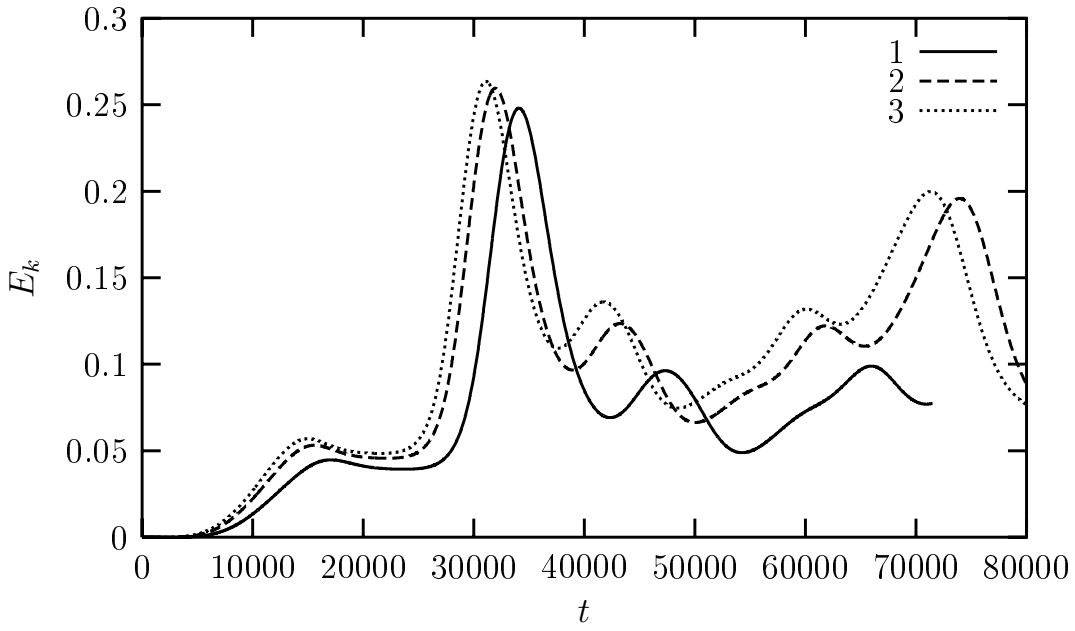

Figure 4.6. Time dependence of flow kinetic energy E_k. 1 — $\sigma_0 = 10^{-4}$, 2 — $\sigma_0 = 2 \cdot 10^{-4}$, 3 — $\sigma_0 = 3 \cdot 10^{-4}$

cessation should occur later. In the next computation, in the same geometry, a conducting layer existed also near the upper electrode with the same conductivity σ_0 as the layer near the blade. Hence, the charge sink existed, and the flow would reach the steady-state regime. Here, a jet of liquid with charge of one sign was observed which ascended from the protrusion along with two oppositely charged descending jets at the vertical borders of the cell. Since the horizontal periodicity, these jets are two parts of one descending jet. The flow between jets consisted of two vortices with opposite signs.

Time evolution of the flow kinetic energy E_k for different values of σ_0 is shown in fig. 4.6. Flow pulsations are readily observable. The cause of them is, that the charge injection leads to the decrease in the electric field on the top of the protrusion thus decreasing the current. When the injected charge moves away from the protrusion, the screening diminishes and the current rises again. Thus, the charge is injected in discrete lumps that are later extended due to liquid motion.

If the voltage between electrodes increases, the main mode of flow becomes unstable. It leads to the growth of small disturbances and the breaking of flow symmetry. Jets shift and distort, additional vortices appear. Figure 4.7 presents the velocity field and the charge distribution at the late stage of flow development. One can readily see complicated flow pattern with several vortices and shifted and distorted charged jets.

The additional contribution to the onset of instability can be made by the

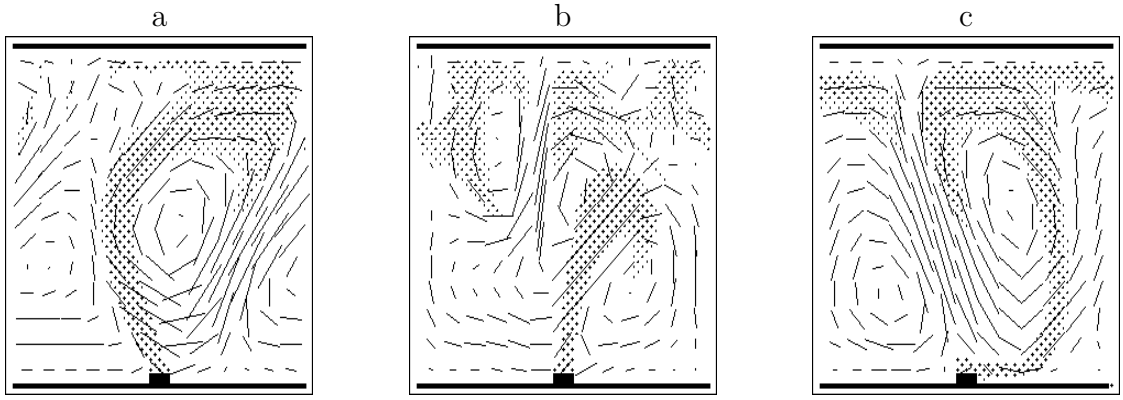

Figure 4.7. Development of EHD flow. Time is $t = 3{,}9 \cdot 10^4$ (a), $5 \cdot 10^4$ (b), $7{,}2 \cdot 10^4$ (c). Shown are the velocity field (lines) and the positive charge density (shades of gray)

strong electric field dependence of the injection current (conductivity of the layer adjacent to an electrode σ_0 is a rapidly increasing function of E). This effect was theoretically considered in [104], it was not taken into account in the present work.

4.4 Generation of vapor bubbles at the electrode surface in high electric field

One of the breakdown inception mechanisms is the bubble one. Bubbles can either pre-exist on the electrodes, or be generated in liquid after the voltage application. After the generation of bubbles, they grow and deform under the electric field action [105–108]. When bubbles achieve a certain size, the conditions for gas breakdown inside them appear. The breakdown of gas inside a bubble leads to a local enhancement of the electric field in a liquid. Under certain conditions, a further breakdown of dielectric liquid becomes possible [109]. For example, for the breakdown of water, the density should become lower than some critical one ($n < n_c$, at that electrons become quasi-free, for water $n_c = 10^{20}$ cm^{-3} [110]), and the bubble size should become sufficiently large for the critical electron avalanche to develop [111].

The generation of vapor bubbles at the initial stages of breakdown of liquids was observed experimentally in [102, 112–114]. Later, the growth of bubbles and the development of EHD-instability on their surface occur leading to the formation of streamer channels (see also chapter 5).

The thermal mechanism of bubble formation is connected with the local heat release in a liquid as a result of the heating by the electric current. When the temperature becomes higher than the boiling temperature of the liquid at a given pressure, the nuclei of vapor bubbles begin to appear which then expand

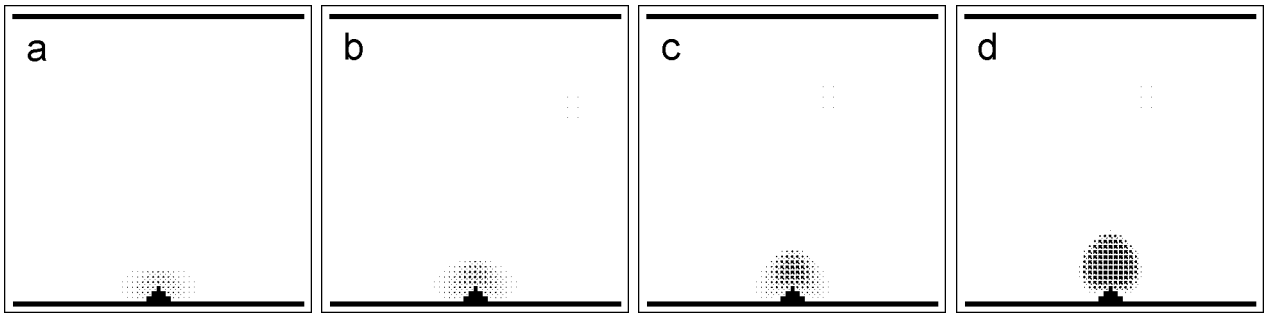

Figure 4.8. Generation and growth of cavitation vapor bubble in high electric field. Time is $t = 80$ (a), 100 (b), 120 (c), 140 (d)

due to the evaporation of new portions of liquid and due to the electric field action. A model was introduced in [111], in that bubble nuclei are formed in the regions of enhanced electric field on microtips by the local heating of liquid due to the field emission [115]. It was shown, that the inception time of the bubble nuclei makes the main contribution to the statistical lag time of a breakdown.

An alternative to the thermal mechanism is the homogenous nucleation of bubbles in the region of low (or negative) pressure even at the initial temperature. Such regions can exist near sharp tips and edges on the electrode surface, where electric field is high enough. This mechanism can be named electrodynamic cavitation. Possibility of bubble generation due to electrodynamic cavitation was mentioned in [8, 112, 116, 117].

When the charge injection from the electrode surface takes place in an electric field, liquid begins to move under the action of electrodynamic forces. At that, compression and rarefaction waves arise in liquid. Regions of low pressure adjacent to electrode appear, in which a phase transition at specified temperature can occur resulting in the generation of vapor micro-bubbles on the electrode surface (cavitation).

To simulate the process of bubble generation, the LBE model with interparticle interaction was used [3, 67] (see also chapter 1) which allows one to simulate phase transition, thus giving the possibility to model directly the process of electrodynamic cavitation. The interparticle interaction should be sufficiently strong $|G| > |G_c|$, and the initial density should be that of the dense phase. The permittivity of liquid ε was considered constant and independent on density (it is possible, if $\varepsilon \approx 1$, an example of such liquid is liquid helium with $\varepsilon = 1{,}05$). Hence, electrostriction forces were not taken into account.

Figure 4.8 presents different stages of the formation and growth of vapor bubble due to electrodynamic cavitation. The density inside the bubble decreased by three orders of magnitude. Thus, for the first time, generation and growth of vapor bubbles in high electric field near the electrode by the electro-

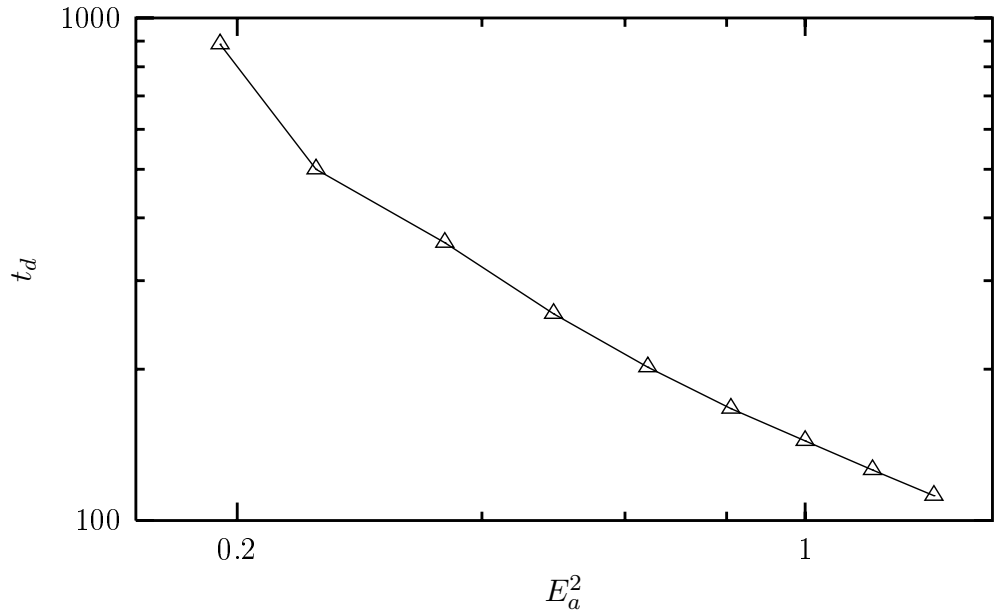

Figure 4.9. Electric field dependence of the bubble development time

dynamic cavitation mechanism was observed in simulations. The breakdown of gas inside bubbles can lead to further breakdown of liquid.

The generation and growth of bubbles at different applied voltages was investigated. Results are shown in fig. 4.9. The time between the voltage application and the generation of a bubble of certain size ($R \approx 5$ lattice units) depended strongly on the electric field strength. This time increased sharply when the electric field decreased. If the field was lower than a certain critical value (in our case $E_{cr} \approx 0{,}44$), the bubble did not appear. Thus, the cavitation mechanism of bubble generation is of the threshold nature.

At higher fields, the development time is approximately inversely proportional to the square of the average electric field E_a ($t_d \sim E_a^{-2}$, fig. 4.9). The same dependence of the development time on the energy release $w = j \cdot E$ was mentioned in [111] for the breakdown of liquid argon and water ($t_d \sim w^{-1}$). In our case, j is proportional to E_a, hence, the energy release is proportional to E_a^2.

The results obtained agree with the conclusions of [102], where the expression for the bubble size vs. time was obtained $R(t) \sim \left(E^2 t\right)^{2/3}$ for the case of viscosity-dominated bubble growth. For fixed R it also leads to $t_d \sim E^{-2}$.

Summary

A lattice Boltzmann equation model for simulation of electrohydrodynamic flows is proposed. Three methods for computation of the convective charge

transport were realized (the method of "LBE-particles", the method of mean velocity, and the method of additional LBE component). Formulas for numeric diffusivity were derived for all methods.

The simulation was carried out of two-dimensional electrohydrodynamic flows caused by the charge injection from a protrusion on the electrode. Under these conditions, a flow of liquid in the shape of a plane vortical dipole is formed. At the initial stage, the flow has strong pulsations caused by the electric field decrease upon the protrusion after the injection of next charge lump. At later stages, the instability of the main flow mode is more significant. The flow symmetry breaks, jets shift and distort, and additional vortices appear.

For the first time, the possibility of micro-bubble generation in high electric field on the electrode surface by the electrodynamic mechanism was confirmed by direct simulations. The electric breakdown of gas in bubbles generated can result then in the breakdown of liquid. The time of bubble development was shown to increase with the decrease in electric field, this effect is of the threshold character. The voltage dependence of the bubble development time was obtained which agrees with theoretical predictions and experimental results.

The method developed is sufficiently simple and effective. It is promising for the simulation of electrohydrodynamic problems.